Spectrochimica Acta Part A: Molecular and Biomolecular Spectroscopy 278 (2022) 121347

Contents lists available at ScienceDirect

Spectrochimica Acta Part A: Molecular and Biomolecular Spectroscopy

journal homepage: www.elsevier.com/locate/saa

Interactions of a biological macromolecule with thermotropic liquid crystals: Applications of liquid crystals in biosensing platform

Priyanki Kalita [a], Ranjan K. Singh [b], Ayon Bhattacharjee [a,*]

[a] Department of Physics, National Institute of Technology Meghalaya, Bijni Complex, Shillong 793003, India
[b] Department of Physics, Banaras Hindu University, Varanasi, Uttar Pradesh 221005, India

HIGHLIGHTS

- Detection of bovine serum albumin (BSA) by 4′-octyl-4-biphenylcarbonitrile (8CB) liquid crystals (LCs)
- Temperature and concentration behaviour of the mixture detected by POM.
- The director configuration of 8CB on addition of BSA showed transition under a POM.
- Detection of BSA by 8CB LC was confirmed at a concentration of 100 μM of BSA.
- Molecular docking and Raman spectroscopy were the novel techniques employed.
- The distribution of binding energy −8.80 Kcal/mol; most favourable docking position is subdomain IB.

GRAPHICAL ABSTRACT

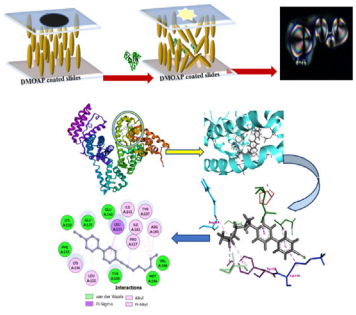

ARTICLE INFO

Article history:
Received 17 January 2022
Received in revised form 8 April 2022
Accepted 1 May 2022
Available online 4 May 2022

Keywords:
8CB
BSA
Liquid crystals
POM
Raman spectra
Molecular docking

ABSTRACT

Liquid crystal biosensor was developed based on a 4′-octyl-4-biphenylcarbonitrile (8CB) by adsorption of biological macromolecule bovine serum albumin (BSA) at the 8CB interface. BSA was detected by examining the changes in the director configurations of 8CB molecules under a polarizing optical microscope. The transitions in the director configuration were due to the non-covalent bonds. This technique demonstrated high sensitivity at a concentration of 100 μM of BSA. The binding events between the 8CB and BSA were investigated through molecular docking studies that confirmed the protein-ligand interaction. The most probable binding location of 8CB to dock with BSA were determined at a subdomain IB of Sudlow's site I. The active residues on analyzing were found to stabilize the 8CB molecules through different interactions. These active residues that were involved in the protein-ligand interaction were further confirmed with Raman spectroscopy. This study provided the vibrational properties and structural changes that occurred due to the various interactions between the 8CB and BSA. The results presented in this work lead to a potential biosensing tool for detecting and sensing proteins using LCs.

* Corresponding author.
E-mail address: ayonbh@nitm.ac.in (A. Bhattacharjee).

https://doi.org/10.1016/j.saa.2022.121347
1386-1425/

1. Introduction

Liquid crystals (LCs) are materials that exhibit different phases due to the interactions between condensed-phase molecules that are orientational subordinate, and noncovalent [1]. The LC molecules have high sensitivity to temperature [2,3], light [4,5], physical and chemical changes on the surface, orientation response, optical anisotropy and low anchoring energy [6-8]. Due to these properties, the utility of LCs to transduce and amplify biomolecular events in terms of optical signals is considered a promising material in the biosensing platform.

Over the recent years, LC-based biosensors have seen significant growth in sensing targets and signal detection methods. These methods are based on the intermolecular and intramolecular interactions, interfacial adsorption that controls the orientational changes in LCs. The characteristics of the output signals upon interactions with foreign substances can be processed, amplified and converted into measurable indicators. LC-based biosensing is monitored based on the orientation of the LC molecules. The detection method is based on the changes in optical images observed under a polarizing optical microscope (POM). This method is used in the adsorption of lipids [9,10], proteins [11-14], surfactants [15] and polymers [16] by LC molecules and amplifies into measurable optical signals. Amin *et al.* reported the detection of biological macromolecules using protein bovine serum albumin (BSA) as probe and LC molecules as signal transducers [17]. Lee *et al.* reported the immunodetection of BSA by dye-doped LCs as a biosensing material for quantitative and qualitative bioassay as in the screening of cancer [18].

The effect of mesophases, namely nematic and smectic phases, interact quite distinctively with the biological macromolecule and changes the alignment of LCs. In the nematic and smectic phases, the formation of droplets is observed only in the presence of biological molecules such as BSA. This results in changes in the phase transition temperature of LCs. When observed under a POM between crossed polarizers, the optical changes show the transition in the director configuration of the LC molecules. The configuration of the LC droplets shows the stability between the elasticity and surface anchoring energy of LCs [19]. The LC droplets with tunable optical properties interact with external stimuli and considerably change their optical appearance [13,20-22]. This results in the transition of the director from radial to bipolar configuration under a POM [13,23-26]. Due to intermolecular and intramolecular interactions, the docking of proteins with LCs plays an essential role in biosensing. This protein-ligand interaction leads to the reorientation of the LC molecules. Vibrational techniques such as Raman spectroscopy give us an insight into the structural changes of various residues of the protein involved in the interaction with LCs [27-29]. Herein, we report the protein BSA detection by LC 4′-octyl-4-biphenylcarbonitrile (8CB). 8CB is selected as it is room temperature LCs and BSA as a probe is selected as albumins are essential to life. The homeotropic alignment induced by surfactant dimethyl octadecyl [3-(trimethoxy silyl) propyl] ammonium chloride (DMOAP) on 8CB LC shows dark optical images under a POM [30].

The novel techniques employed are molecular docking and temperature-dependent Raman spectroscopy. These techniques used in our research work are not reported elsewhere before in the detection of proteins by LCs. On increasing the BSA concentrations, the orientation of the LC director tends to change from homeotropic to planar, accordingly. This change results in the detection of BSA at a particular concentration by 8CB during their crystalline to isotropic phase. The binding properties of the BSA and 8CB are further investigated with protein–ligand interaction with detailed docking studies. The vibrational properties of the active residues of BSA involved in the binding with 8CB are examined by temperature-dependent Raman spectroscopic studies. These techniques are employed to detect BSA by 8CB LC with the potential to develop a simple, sensitive, and cost-effective LC-based biosensor.

2. Experimental section

2.1. Materials

The compounds DMOAP and 8CB LC were procured from Sigma-Aldrich. BSA (05470) was purchased from HiMedia. They were utilised without further purification. The different phases transitions of 8CB from a crystal (K)-smectic A (SmA)-nematic (N)-isotropic (I) is shown in Fig. 1 [31]. The phase transition temperatures and textures of pure 8CB under a POM were examined and found to agree with the literature [31-33]. The protein BSA is a heart-shaped structure, having 583 amino acids [34,35]. BSA free of fatty acids was prepared in phosphate-buffered saline (PBS) explained in the literature [12]. The protein concentration was determined with an extinction coefficient of 43,800 M^{-1} cm^{-1} at 280 nm [36,37]. The determination was employed by adsorption measurements using a UV–Vis spectrophotometer (Shimadzu UVPC 2450 Corporation, Tokyo, Japan).

2.2. Methods

2.2.1. Preparation of DMOAP coated glass slide

DMOAP is a surfactant that possesses a long alkyl chain. The surface coupling agent has strong LC orienting interaction and is predicted to have the permanence necessary for long device lifetimes due to its chemical stability [38]. DMOAP facilitates absorption, induces homeotropic alignment at the surface and produces a dark background under crossed polarizers. DMOAP solution was prepared by dissolving 1% (v/v) of DMOAP solution in 100 mL of deionized (DI) water. The cleaned slides were baked for 15 min at 80 °C (Fig. 2(a)). After drying, the slide is coated with DMOAP (1% v/v) and kept undisturbed for 15 mins. The unbound DMOAP solution was then washed off the slides with DI water. The last step was to these coated slides under a stream of nitrogen gas and baked again at 80 °C to form a self-assembly layer shown in Fig. 2(b).

2.2.2. Fabrication of 8CB-BSA cells

After earlier steps followed in treating the surface of glass slides with DMOAP, a cell was formed by placing a square-shaped Mylar spacer of 12 μm thickness with an opening on one side. 8CB was injected into the cell with the help of a syringe between the two coated slides. The optical texture under a POM was observed, and the homeotropic alignment of LCs was validated from Fig. 2

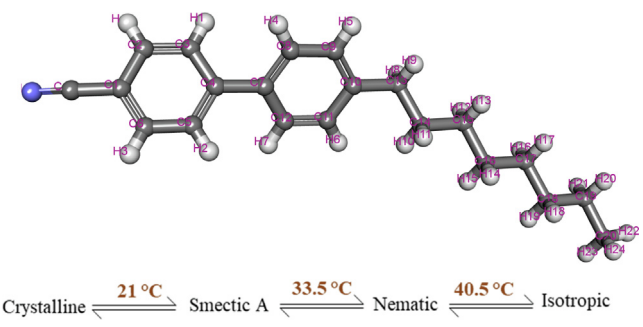

Fig. 1. Optimized molecular structure for 4′-octyl-4-biphenylcarbonitrile (8CB).

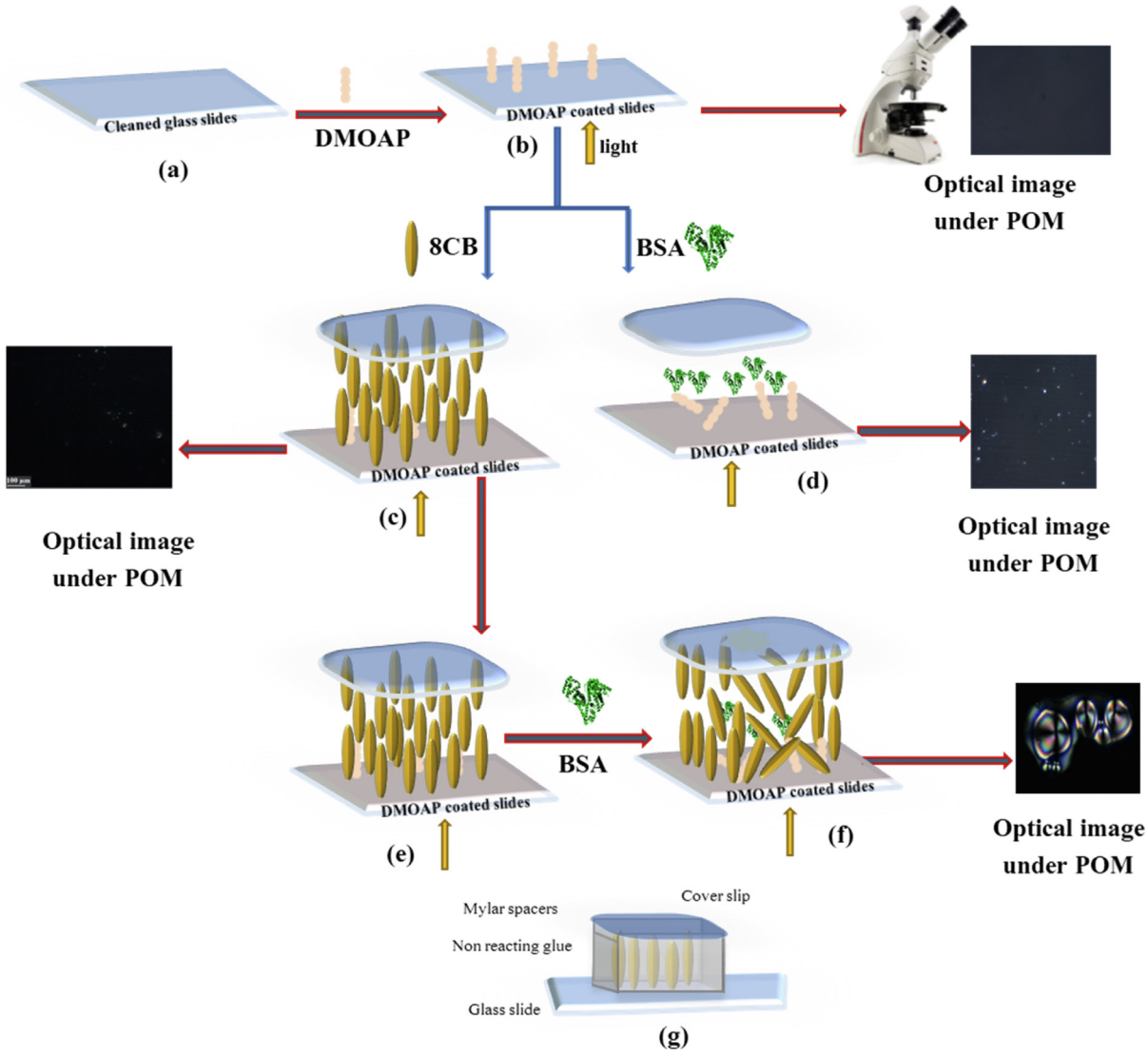

Fig. 2. Schematic presentation of LC-based cell to develop a biosensor with the preparation of (a) cleaned glass slide, (b) DMOAP coated glass slide (c) DMOAP modified 8CB slide (d) DMOAP modified BSA slide (f) introduction of BSA on (e) DMOAP modified 8CB glass slide, (g) schematic illustration of LC cell describes in section 2.2.2.

(c). Next, the target molecule protein BSA was introduced into the cell through an inlet. The initial amount of protein (50 μM, 80 μM, 100 μM, 300 μM, 600 μM) BSA was introduced into 8CB LC at the DMOAP modified 8CB LC interface to study the detection and interaction between them. The POM images on the introduction of BSA to the DMOAP treated surface shows a black texture, as shown in Fig. 2(d). These studies the alteration in the morphology of 8CB in the presence of BSA (Fig. 2(f)). It is to be noted that a glass coverslip was placed on top of the sample to create uniformity of samples, as in Fig. 2(g). Two types of cells: 8CB filled cells without BSA as the control (Fig. 2(c)), and 8CB filled cells with BSA to investigate the effect of protein-LC interaction (Fig. 2(f)).

2.2.3. Determination of the orientation of 8CB by polarizing optical microscopy with detection of BSA

The orientation of 8CB LC on protein complex was observed using a Leica DM2700P (Germany) POM. A thermal stage (LTS420, Linkam, UK) with a temperature controller mounted on the POM was used. The POM was used with crossed polarizers in the transmission mode in the absence of transmitted light during a 360° rotation of the stage. The LC cell was placed on a thermal stage of POM. The POM was set at a 10 × objective to observe the morphological changes under crossed polarizers. The studies were conducted in two domains. First morphological variations with temperature and secondly with concentration. The temperature-dependent studies were performed to determine the orientational changes in LC molecules. These temperature-dependent studies were conducted for both the control cells as well as the BSA-filled cells to eliminate the effects of LCs. The homeotropic alignment was confirmed by an interference pattern of two crossed isogyres. The images at selected locations were obtained with a camera by Leica (MC170 HD) mounted on the microscope at a magnification of 10×. The concentration-based studies were performed in order to sense and verify the optical changes observed due to the BSA interaction with 8CB. The optical images were determined to detect albumins at a particular concentration of BSA.

2.2.4. Determination of the binding sites and the ligand-protein interaction through molecular docking

The computational study involves the *in-silico* investigation of the intermolecular interaction between a receptor and ligand. The protein BSA, which consists of 585 amino acid residues, is selected as a receptor [PDB ID: 4F5S] having chain A. The 3D struc-

tures are obtained from Protein Data Bank (https://www.rcsb.org/) [39] in PDB format. The liquid crystal 8CB used as a transducing element was selected as a ligand for docking with receptor BSA. The 3D structure of 8CB LC was obtained from PubChem (https://pubchem.ncbi.nlm.nih.gov/)[40] in the extension of.mol file format. The Blind Docking Server available at https://bio-hpc.eu/software/blind-docking-server/ [41] was used to determine the active amino residues for docking with LC molecules [42]. The docking analysis was further performed with Discovery studio visualizer 2020 from BIOVIA. Molecular docking aims to predict the ligand to interact with the protein at the atomic level that allows to determine the behaviour of the ligand in the binding sites of proteins. Two basic steps are required: prediction of the ligand confirmation and its position and orientation within these sites and evaluation of the docked site of the selected cluster via different interactions [43,44]. This section focuses on calculating molecular interactions, the docked conformers, scoring and evaluating docked ligands and proteins.

2.2.5. Vibrational studies of the interaction through Raman spectroscopy

The 8CB interaction with BSA was studied by Raman spectroscopy with 100 μM BSA concentration, as confirmed from the POM studies. The spectra were recorded using an inVia Raman spectrometer from Renishaw (UK), equipped with 532 nm lasers and a cooled charged coupled device detector. The samples were placed in a small well 15 mm in diameter in a quartz sample holder. The plate is then mounted on a THM 600 Linkam hot-stage. The calibration of the system was done by recording the spectra at 520 cm^{-1} using silicon reference. Laser power was restricted to 5 mW to avoid laser heating of the sample. The sample was observed under a Leica DM 2500 M microscope attached with the instrument and focused with a magnification of 50 × long-dis tance objective. The laser lines with a slit width of 50 μm were maintained throughout the measurement. The data was recorded with 100 scans averaging to obtain accurate results. The spectral parameters, namely, the peak position (PP), line-width (LW), and the integrated intensity (II), are measured accurately by Lorentzian fitting. The deconvolution and fitting of the curves were achieved using the Thermocon GRAMS AI version 9.3 suite from Thermo Fischer Scientific. It is a Windows-based suite of powerful yet intuitive software tools for analyzing and processing spectral data.

3. Results and discussions

3.1. Textural studies under polarizing optical microscopy

The polarized optical images of the changes in the DMOAP modified 8CB in the presence of BSA are investigated under a POM, observed in Figs. 3-7. The optical textures of pure 8CB and pure BSA on a DMOAP coated surface are shown in S.I. Fig. 1. The molecules of the surfactant coated on the surface significantly impact the LC molecular orientation. So, it is an important factor to investigate the behaviour of the mesogen on modification by surfactant DMOAP. 8CB molecules are hydrophobic in nature and do not attach to the surface independently. Due to the long alkyl hydrocarbon and flexible chains of DMOAP, 8CB molecules readily adheres to the DMOAP treated surface, as shown in Fig. 2(c) without BSA. DMOAP facilitates the formation of naturally spherical 8CB droplets of radial configuration after allowing it to settle for some time at room temperature. DMOAP induces homeotropic alignment of the LCs when no hydrogen bond is present. It stimulates coordination [45,46] between the treated surface and the 8CB molecules. Dark background in optical images is observed due to the perpendicular alignment of 8CB molecules. On addition of BSA to the 8CB treated surface, changes in the orientational ordering of the molecules occur, which are observed as textures. By increasing the concentration of BSA, major changes in texture are observed that are analyzed further.

The 8CB droplets on interaction with 50 μM of BSA in Fig. 3 show that the phase transition from K to SmA is found to be shifted from pure 8CB LC by 3 °C. The texture for the SmA phase at 31.9 °C is shown in Fig. 3(b). The phase transition from SmA to N is at 32.4 °C, and the texture for the N phase is presented in Fig. 3(c) at 38.5 °C. The visual appearances of LCs show the formation of 8CB droplets at 80 μM of BSA when there is a phase transition from SmA-N. The droplets start appearing at the temperature of 38.4 °C (Fig. 4). The textures at the different regions are shown in S.I. Figs. 2-3.

The K-SmA phase transition temperature of 8CB droplets, in addition to 100 μM BSA, is observed at 21 °C shown in Fig. 5. The droplets show the radial configuration, and the same droplets change their orientation to the twisted radial configuration at the SmA-N phase and bipolar at the N phase. The same region also shows the schlieren texture at the N phase, denoting homeotropic changes to planar alignment at the LC surface. This confirms that the detection of BSA by 8CB is possible at this concentration as the orientation changes from homeotropic to planar.

For better results, we further increase the concentration of BSA to 300 μM. The K-SmA phase transition occurs at a temperature of 23 °C and SmA-N at 32.6 °C, where the 8CB droplets show the radial configuration. On considering a particular area for the better visualization of the droplets, a pre radial to escape radial configuration of the droplets is observed as seen from Fig. 6(b)-(c). The same droplet changes into the bipolar configuration as in Fig. 6 (d). The change in a radial to the bipolar configuration of the droplet occurs due to adsorption of BSA at DMOAP modified 8CB surface. If the concentration is further increased to 600 μM, in that case, we see that the transition in the droplets is from radial to twisted radial, twisted-radial to pre-radial and then to bipolar configuration. These configurational changes occur during the N-I

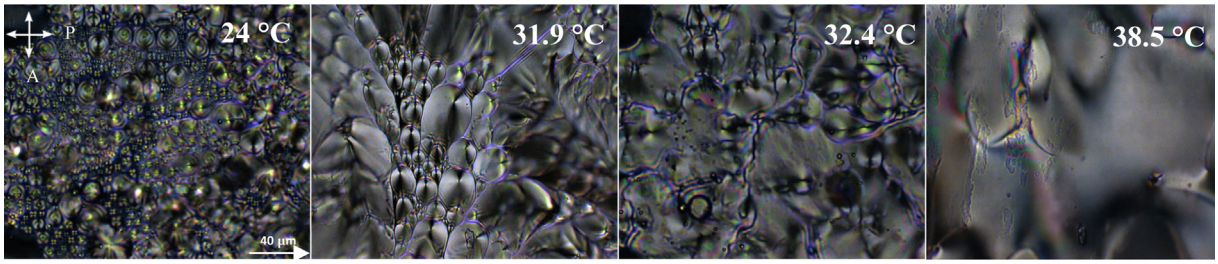

Fig. 3. Crossed polarized optical images of DMOAP modified 8CB LCs exhibited changes during the phase transition from K-I on exposure to BSA at a concentration of 50 μM. Scale bars: 40 μm.

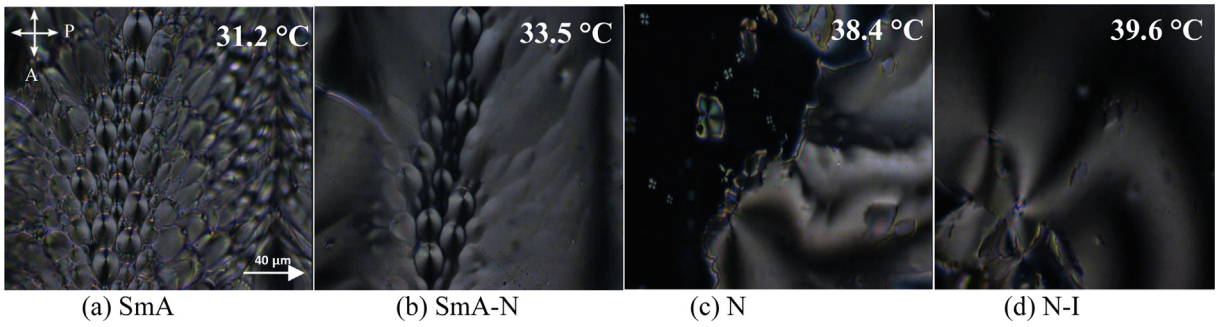

Fig. 4. Crossed polarized optical images of DMOAP modified 8CB LCs exhibited changes during the phase transition from K-I on exposure to BSA at a concentration of 80 µM. Scale bars: 40 µm.

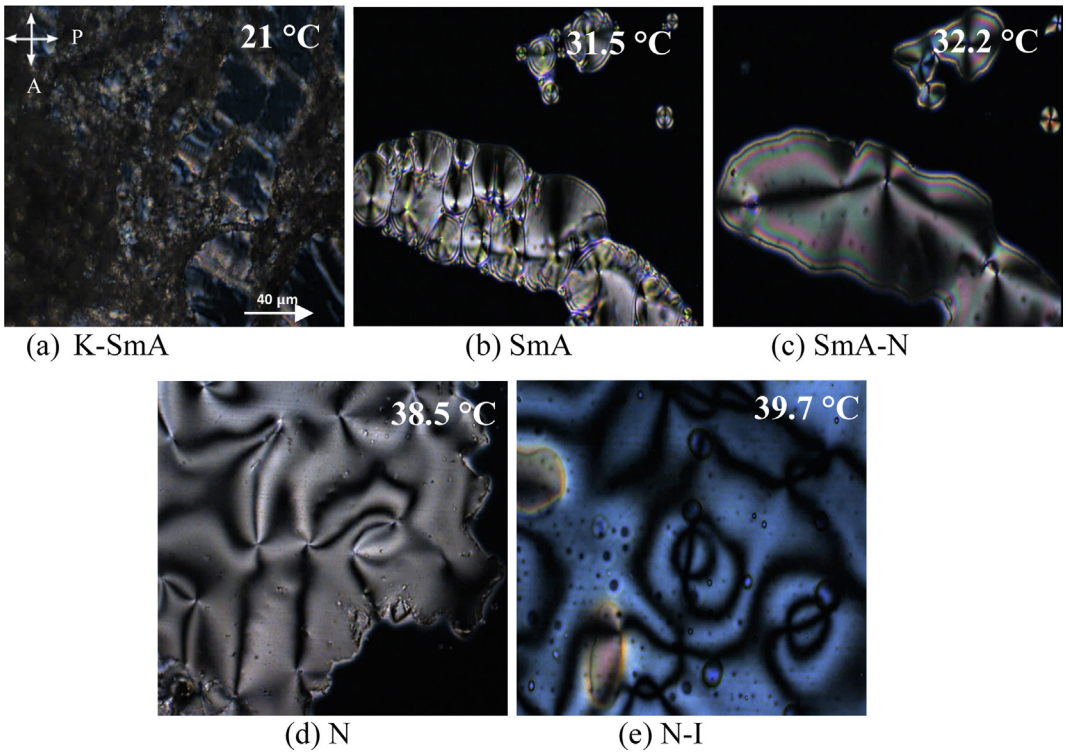

Fig. 5. Crossed polarized optical images of DMOAP modified 8CB LCs exhibited changes during the phase transition from K-I on exposure to BSA at a concentration of 100 µM. Scale bars: 40 µm.

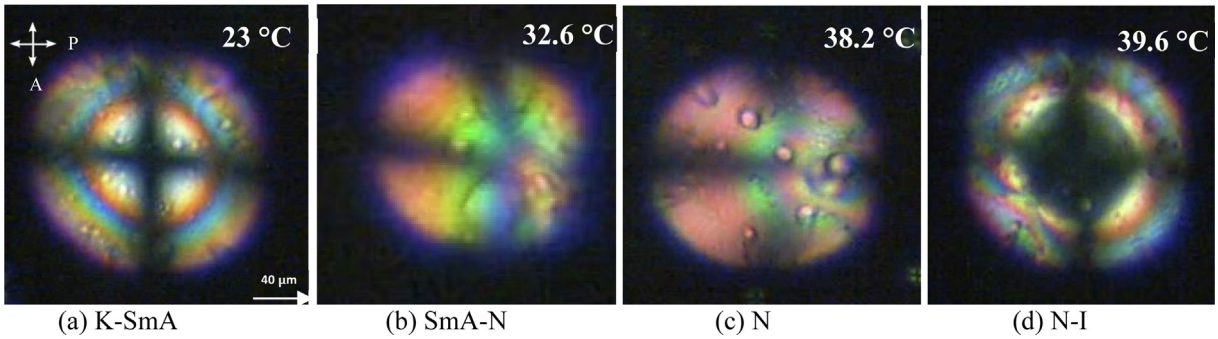

Fig. 6. Crossed polarized optical images of DMOAP modified 8CB LCs exhibited changes during the phase transition from K-I on exposure to BSA at a concentration of 300 µM. Scale bars: 40 µm.

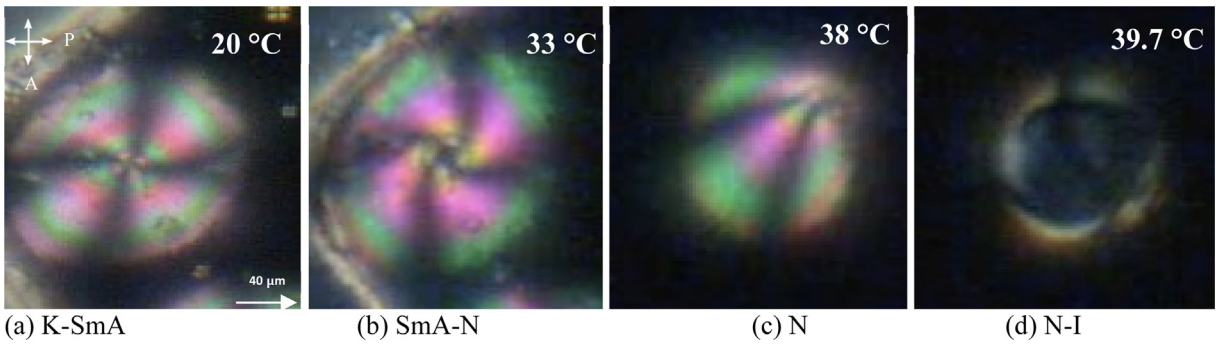

Fig. 7. Crossed polarized optical images of DMOAP modified 8CB LCs exhibited changes during the phase transition from K-I on exposure to BSA at a concentration of 600 μM. Scale bars: 40 μm.

phase transitions (Fig. 7). The N phase at different regions is shown in S.I. Figs. 4-5.

Whenever the concentration of BSA has dropped below 100 μM, the transfiguration of the director and the orientation of the droplets does not occur. The considered concentrations of BSA shows that the limit of BSA to be detected by 8CB LC is at a concentration of 100 μM. The detection limit is based on the phase and a specific time frame when the droplets show the transition from radial (homeotropic) to bipolar (planar) configuration.

Based on the interfacial adsorption of BSA due to the interactions between BSA and 8CB, POM shows changes in the form of optical signals. Thus, the hydrocarbon alkyl chains play a vital role in the adsorption of BSA. The binding behaviour, such as the electrostatic interactions like van der Waals interactions, interfacial interactions like hydrogen bonding, plays an essential role in LC-based biosensing. The hydrophobic, hydrogen bond and non-covalent interactions help provide insights into the radial to the bipolar configuration of the LCs. Thus, LC biosensing can be implemented based on the detection of BSA at a specific limit of concentration by 8CB droplets.

3.2. Molecular docking

Molecular docking is an *in-silico* method that determines the interactions and the docked poses of 8CB with BSA. Molecular docking has developed to be an essential technique in drug development for contributing structural information about protein-ligand interaction. This method can be used to characterize the interaction between a small molecule such as LC and the binding site of the target receptor such as proteins. The possible binding poses between ligand and receptor are significant due to the six degrees of freedom including translational, and rotational. However, the lowest binding energy of all the possible poses is selected as the best pose for further studies. This docking incorporates Monte Carlo simulations to model the flexible ligand while the receptor remains rigid. Monte Carlo method generates ligand poses through rigid body rotation, bond rotation or translation [47,48]. This method also explains the basic biological and chemical techniques. The scoring function [49], which determines the energy for the ligand-receptor interaction in a system, calculates the hydrophobic, hydrogen bonds and van der Waals terms. This scoring function is based on the optimized potential for liquid simulations (OPLS) force field [50]. The receptor and ligand optimization are done using PLIP version v1.3.2 [51]. The obtained clustered poses include non-overlapping poses with the best affinities and lowest scoring function. The clustered affinities and interactions contain the images depicting and files representing the interactions between the ligand and active residues.

The binding Sudlow's sites I and II of BSA (situated in subdomain IIA and subdomain IIIA, respectively) [34] are divided into three domains and subdivided into six subdomains. The possible ligand-binding regions with protein BSA are in subdomains IA, IB, and IIA [35]. The docking analysis shows that the 8CB is bonded to the subdomain IB of site I surrounded by active residues of BSA, as shown in Fig. 8(b). The binding energy required by 8CB to bind with BSA is determined to be −8.80 Kcal/mol at subdomain IB. The binding site selection is determined with the energetic contribution to the lowest binding energy and highest binding affinity among all the calculated poses (Fig. 8(c)). The energetic contributions to the binding energy are shown in Fig. 9.

A graph with the breakdown of the binding energy of the best cluster having binding energy −8.80 kcal/mol into the different contributions is shown in Fig. 9(a) and energetic contributions for each atom in the ligand 8CB in Fig. 9(b). Fig. 8(d) shows the binding of 8CB with active residues of BSA, namely Leucine (LEU) 115, Proline (PRO)117, LEU122, Glutamic acid (GLU)125, Lysine (LYS)132, Phenylalanine (PHE)133, LYS136, Tyrosine (TYR)137, GLU140, Isoleucine (ILE)141, TYR160, ILE181, Arginine (ARG)185, Methionine (MET)184 and Valine (VAL)188.

Fig. 8(c) shows the residues of BSA stabilize the biphenyl ring of 8CB liquid crystal through π-alkyl, π-sigma, and alkyl interactions, The C-atom of LEU122 and LYS136 of BSA stabilize the phenyl ring (A) of 8CB through π-alkyl interactions. The C-atom of LEU115 stabilizes the phenyl ring (B) of 8CB through π-sigma interactions. The secondary amine nitrogen, i.e., NH_2^+ present in PRO117, stabilizes the phenyl ring (B) of 8CB through π- alkyl interactions. The same PRO117 also stabilizes the C-atom of 8CB through alkyl interactions. The CH_3 of the ILE181 and C-atom of ARG185 stabilize the C-atom of 8CB through alkyl interactions. The CH_3 group of ILE141 establish alkyl interactions to stabilize the C-atom of 8CB LC. The benzene ring of TYR137 binds with 8CB through π-alkyl interactions. Also, the residues GLU125, LYS132, PHE133, GLU140, TYR160, MET184 and VAL188 stabilize the atoms of 8CB through van der Waals interactions.

The residues LEU115, PRO117, LYS136 and ARG185 of BSA and the cyano group of 8CB act as the solvent-accessible surface area (SAS) for the protein-ligand interaction as shown in Fig. 10(a). Hydrogen bond donors and bond acceptors are examined during the interaction. The cyano group of 8CB molecules, LYS136 and ARG185, have the lowest hydrophobicity region. In contrast, the LEU115, ILE181 and phenyl rings of 8CB have the highest hydrophobicity region of value + 3. The hydrophobicity pocket with the interacting residues is shown in Fig. 10(b). The residues LYS136 and ARG185 of BSA, cyano group and phenyl rings of 8CB LC are in the donor region, as shown in Fig. 10(c). The π interactions involved in the binding process of 8CB and BSA involves the negatively charged π-electron cloud of residues and positively

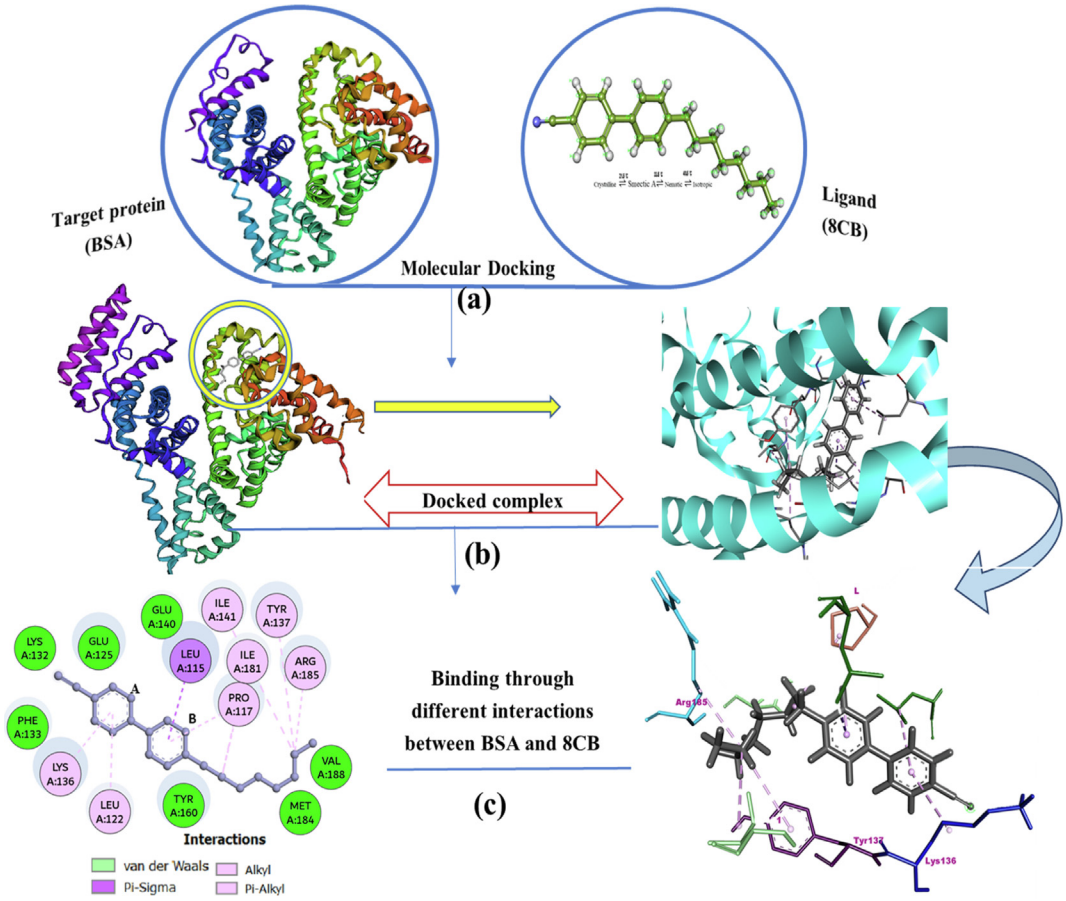

Fig. 8. Schematic illustration of the molecular docking of (a) protein–ligand: BSA on 8CB LC, (b) docking of 8CB and BSA with the best pose and location; with the (c) 2D and 3D diagram of the active residues of BSA binding with 8CB molecules through different interactions [43].

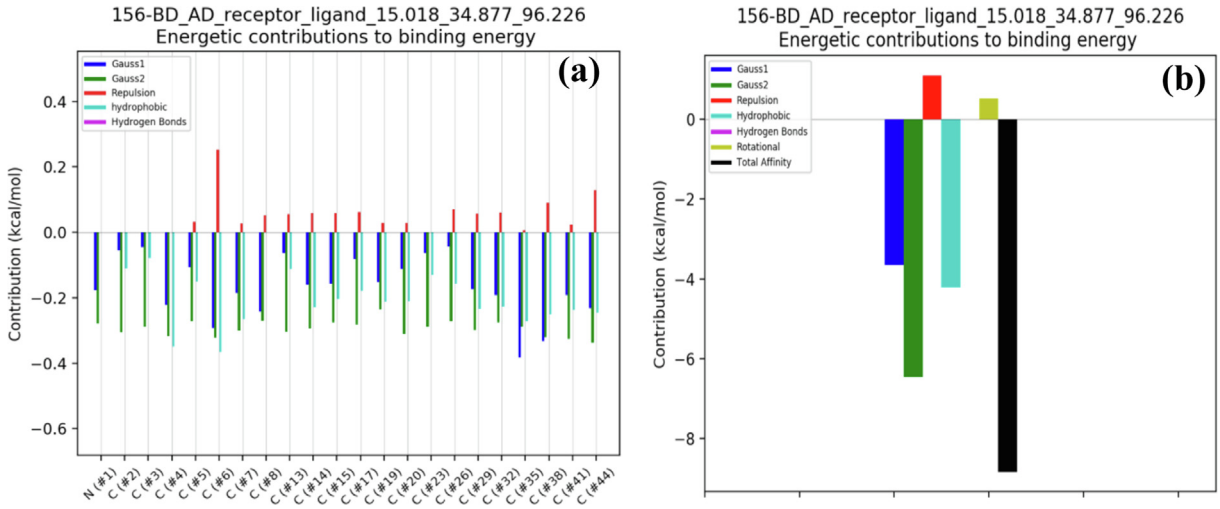

Fig. 9. Energetic contributions to the binding energy (a) breakdown of the binding energy of the best cluster of the receptor, (b) energetic contributions for each atom in the ligand.

charged σ framework of the neighbouring residues or molecules. The positively charged residues of BSA are LYS136, ARG185 and cyano group of 8CB interact with negatively charged residues LEU122 and ILE141 of BSA as evaluated from Fig. 10(d). The docking analysis confirms the binding of 8CB with BSA through non-covalent interactions as obtained during optical studies. Further studies with Raman spectroscopy are performed to confirm the active binding residues of BSA and their interactions with 8CB molecules and to study their structural changes. The detailed information of the residues involved in the interaction with the ligand is listed and summarized in Table 1.

3.3. Vibrational studies through Raman spectroscopy

Raman spectroscopy is an emerging tool to study the vibrational fingerprints of the interaction between the LC 8CB and pro-

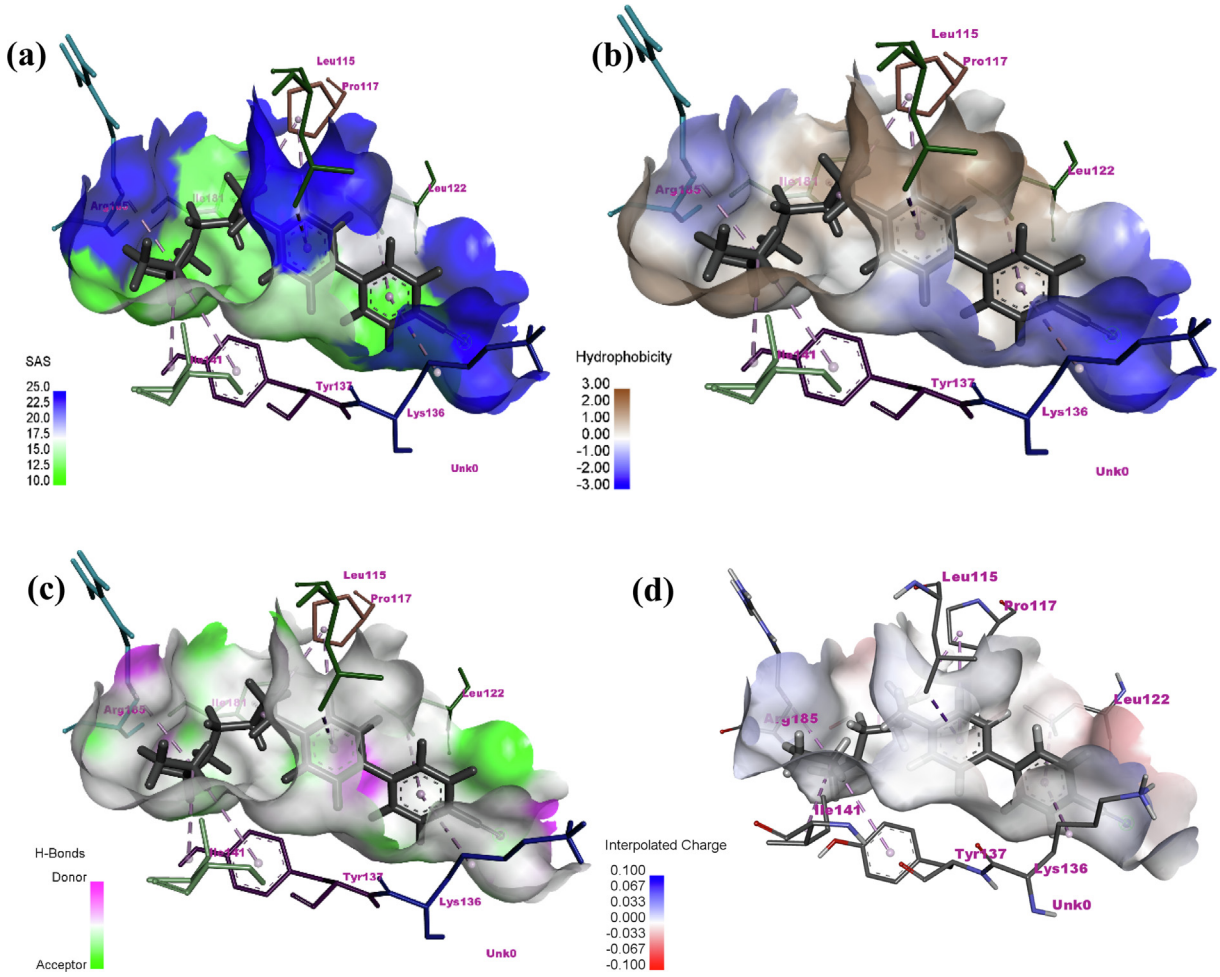

Fig. 10. Docking of 8CB LC with BSA where the receptor surfaces show (a) SAS, (b) hydrophobicity region, (c) hydrogen bond, (d) Interpolated charge.

Table 1
Detailed analysis of the BSA residues involved in BSA-8CB interaction.

Residue No.	Residue Type	Residue Chain	Distance (Å)
115	Leucine (LEU)	A	3.53
122	Leucine (LEU)		3.84
133	Phenylalanine (PHE)		3.39
136	Lysine (LYS)		3.62
136	Lysine (LYS)		3.95
137	Tyrosine (TYR)		3.69
137	Tyrosine (TYR)		3.54
141	Isoleucine (ILE)		3.60
181	Isoleucine (ILE)		3.54
185	Arginine (ARG)		3.69
188	Valine (Val)		3.54

Residue No.	Residue Type	Residue Chain	Centre Distance (Å)		Angle (°)
		Hydrogen Bonds	H-A	D-A	
125	Glutamic acid (GLU)	A	2.81	3.65	66.53

tein BSA. The formation of the protein-ligand interaction is an essential step in biosensors. From the POM and docking analysis, the detection of BSA by 8CB is shown in the previous sections. But their structural changes that take place during these interactions are yet to be discussed. Therefore, temperature-dependent Raman spectra in the region of 400–4000 cm^{-1} are recorded. The temperature under which this study is performed is in the range of −50 °C to 45 °C at a concentration of 100 μM BSA. The spectral region for better visibility is parted into three viz. 400–1000 cm^{-1}, 1000–2000 cm^{-1} and 2000–3300 cm^{-1} as shown in Figs. 11-13, respectively. The variation of Raman parameters with temperature in Figs. 11-13 is calculated and plotted from Figs. 14-21. These

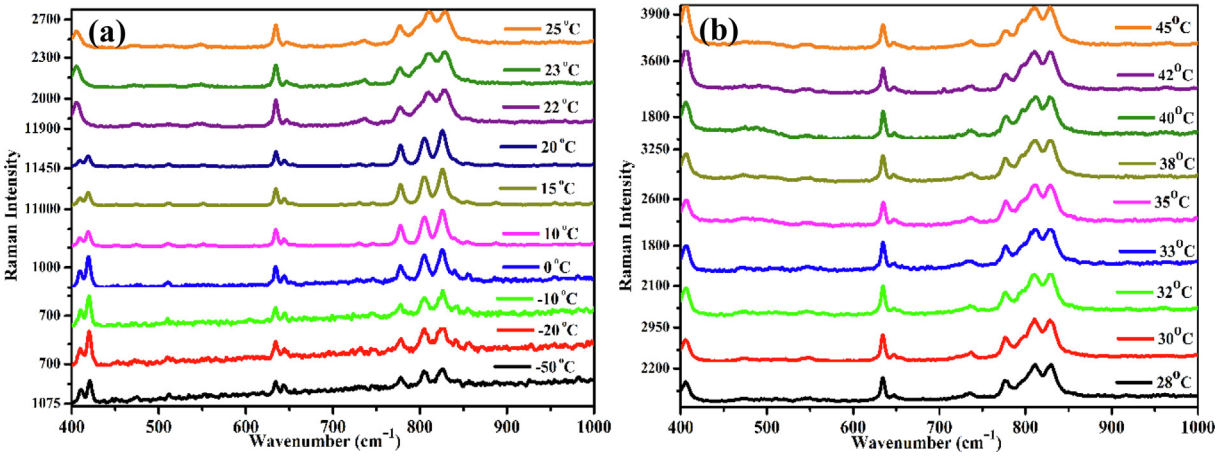

Fig. 11. Temperature-dependent Raman spectroscopic in the spectral region 400–1000 cm^{-1} for the temperature ranging (a) −50 °C to 25 °C and (b) 28 °C to 45 °C.

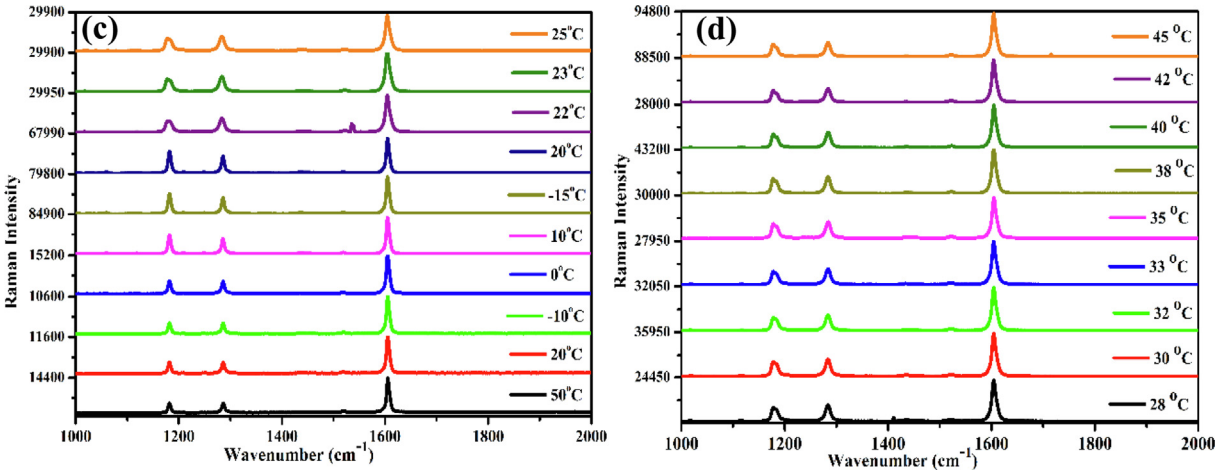

Fig. 12. Temperature-dependent Raman spectroscopic in the spectral region 1000–2000 cm^{-1} for the temperature ranging (c) −50 °C to 25 °C and (d) 28 °C to 45 °C.

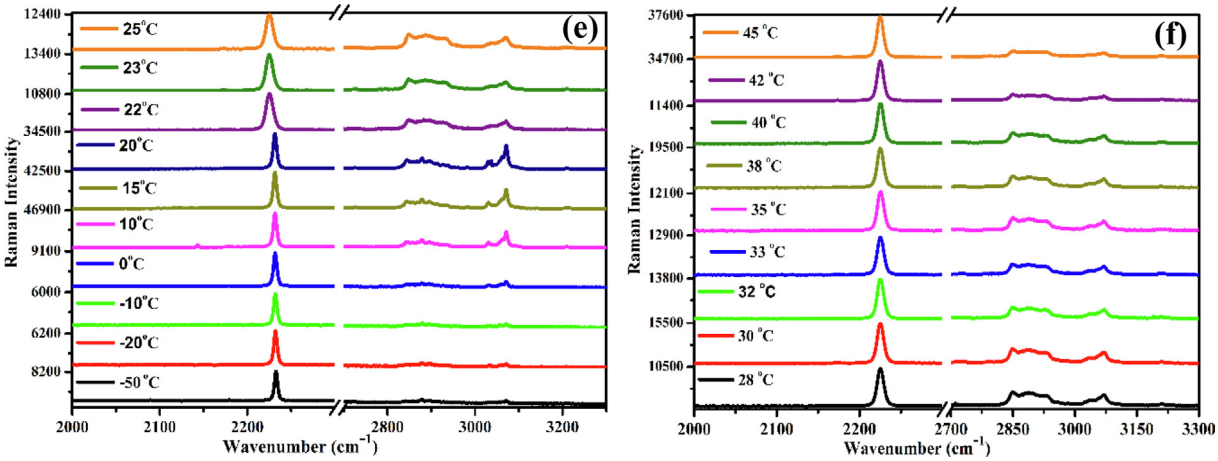

Fig. 13. Temperature-dependent Raman spectroscopic in the spectral region 2000–3300 cm^{-1} for the temperature ranging (e) −50 °C to 25 °C and (f) 28 °C to 45 °C.

parameters provide information about the structural changes of molecules that arise due to the interaction between 8CB and BSA. The notable changes are observed mainly during the phase transitions of 8CB molecules. Below are the Raman spectra for the temperature range −50 °C to 45 °C divided into two segments −50 °C to 25 °C and 28 °C to 45 °C. The following sections can determine the essential features of the interactions and their assignments.

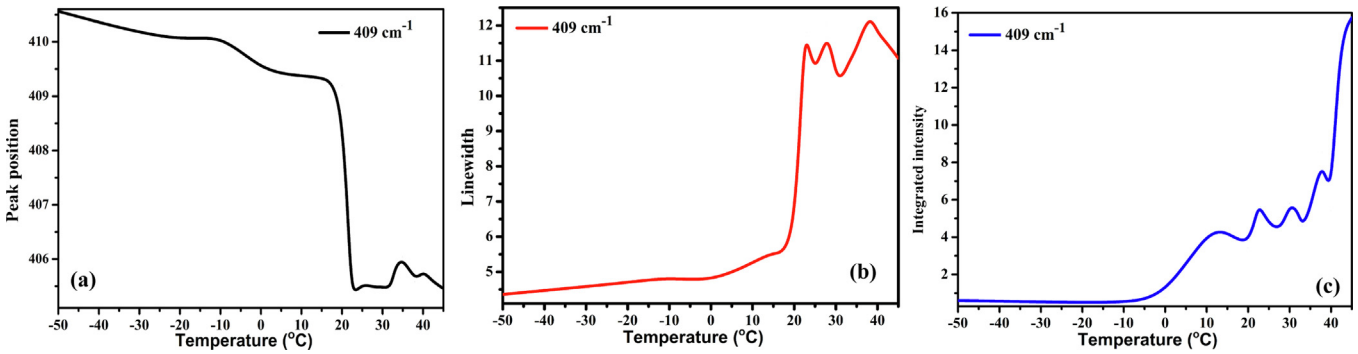

Fig. 14. Variation of Raman parameters (a) peak position, (b) line-width, and (c) integrated intensity for the peak at 409 cm^{-1} with temperature ranging from −50 °C to 45 °C.

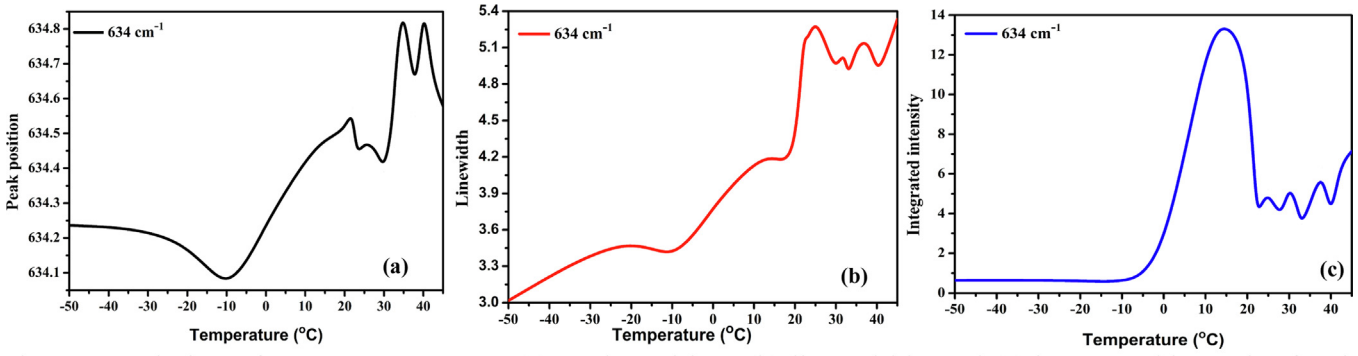

Fig. 15. Variation of Raman parameters (a) peak position, (b) line-width, and (c) integrated intensity for the peak at 634 cm^{-1} with temperature ranging from −50 °C to 45 °C.

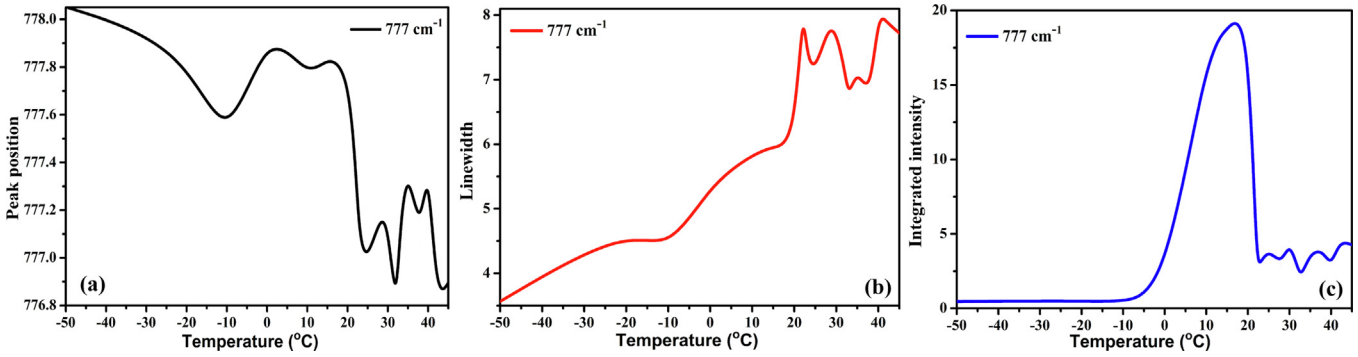

Fig. 16. Variation of Raman parameters (a) peak position, (b) line-width, and (c) integrated intensity for the peak at 777 cm^{-1} with temperature ranging from −50 °C to 45 °C.

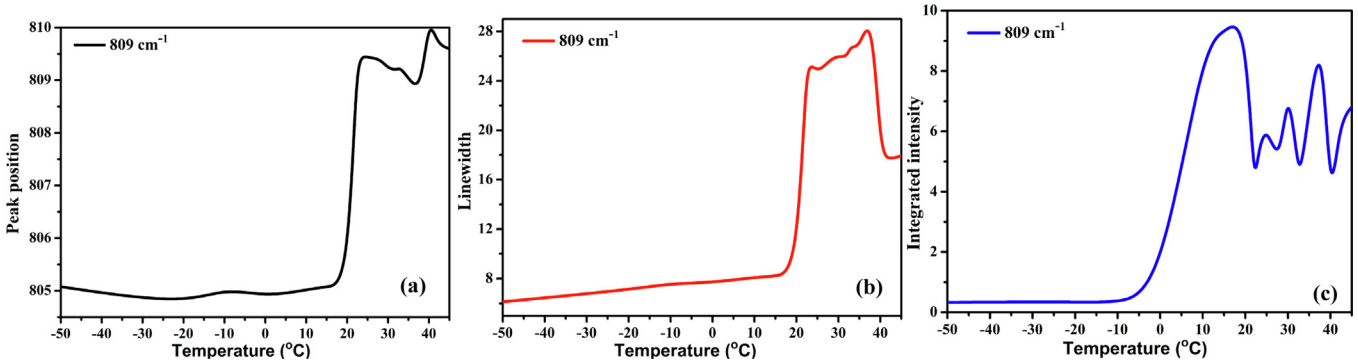

Fig. 17. Variation of Raman parameters (a) peak position, (b) line-width, and (c) integrated intensity for the peak at 809 cm^{-1} with temperature ranging from −50 °C to 45 °C.

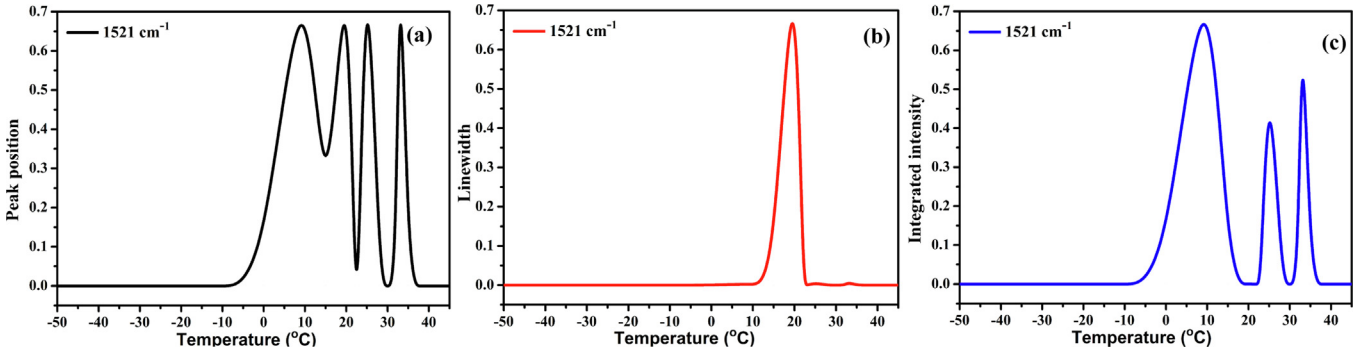

Fig. 18. Variation of Raman parameters (a) peak position, (b) line-width, and (c) integrated intensity for the peak at 1521 cm^{-1} with temperature ranging from −50 °C to 45 °C.

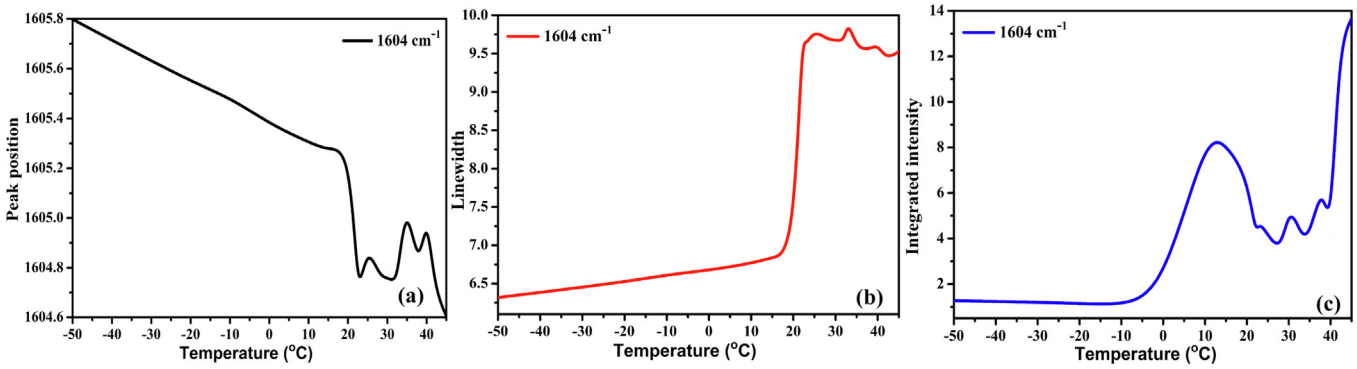

Fig. 19. Variation of Raman parameters (a) peak position, (b) line-width, and (c) integrated intensity for the peak at 1604 cm^{-1} with temperature ranging from −50 °C to 45 °C.

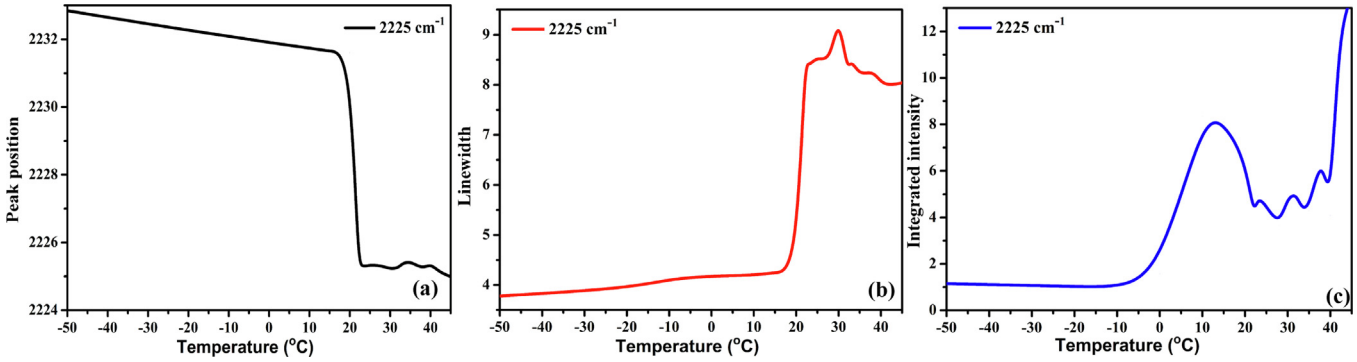

Fig. 20. Variation of Raman parameters (a) peak position, (b) line-width, and (c) integrated intensity for the peak at 2225 cm^{-1} with temperature ranging from −50 °C to 45 °C.

The interaction between protein BSA and LC 8CB show the Amide bands I, II and III. These bands arise due to the bond vibrations in the albumins.

3.3.1. Raman parameters in the spectral region of 400–1000 cm^{-1}

In the spectral region of 400–1000 cm^{-1}, the prominent peak at 409 cm^{-1} is assigned to the υ(S-S) in albumin of BSA. The different assignments for Raman bands have been allocated and are listed in Table 2. The peaks at this region disappear into one peak at a temperature of 22 °C, i.e., at K state observed in Fig. 14. The peak at 634 cm^{-1} is assigned to the υ(C-H) of the benzene ring of PHE on binding with 8CB C-atoms. Another peak at 648 cm^{-1} is assigned to the TYR residue of BSA [52]. The docking analysis also confirms that the PHE and TYR residue of BSA attaches to a C-atoms and phenyl ring of 8CB, respectively. The peak 648 cm^{-1} appears during the SmA-I phase transition of 8CB, and the peak 808 cm^{-1} is attributed to the υ(C-C) of 8CB.

The Raman parameters, namely PP, LW and II varying with temperature for this spectral region, are shown in Figs. 14-17. The peak at 409 cm^{-1} and 777 cm^{-1} shift their position by 4 cm^{-1} during the SmA-I phase transition of 8CB. The peaks at 634 and 809 cm^{-1} shift from lower to a higher frequency during the K-I phase transition. The reason for the decrease in PP the bond either breaks down due to decreased energy. The LW of these peaks shows a sharp increase with an increase of temperature, the natural lifetime is short. The spectral parameters show the LW increases in the SmA-N phase transition. This analysis gives an indication that the lower the temperature better is than the detection process. Due

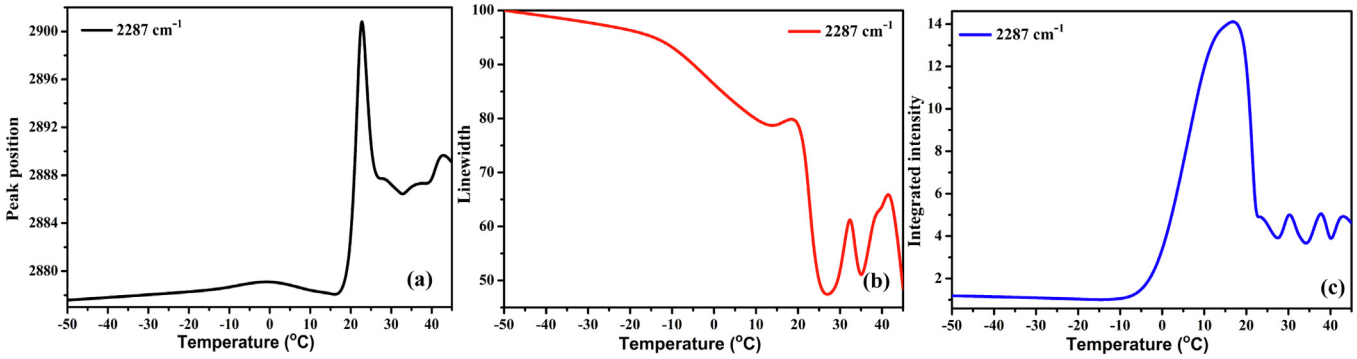

Fig. 21. Variation of Raman parameters (a) peak position, (b) line-width, and (c) integrated intensity for the peak at 2287 cm^{-1} with temperature ranging from −50 °C to 45 °C.

Table 2
Raman band assignment for the Raman peaks of pure 8CB, pure BSA, and their interactions.

Pure 8CB (Δν) cm^{-1}	Pure BSA (Δν) cm^{-1}	Band assignment for pure 8CB	8CB bonded with BSA (Δν) cm^{-1}	Band assignment for docking of 8CB-BSA complex
–	–	–	405	Out-of-plane vibrations of the benzene ring
639	622	Ring vibration	634	The TYR of BSA binds with the phenyl ring of 8CB
-	-		648	
780	777	Ring breathing vibration	777	Ring breathing vibration δ(CO_2^-) from LEU
806	800	Ring breathing vibration	809	Ring breathing vibration with TYR residue of BSA; υ(C-C) of 8CB
826	825	Alkyl chain vibration	829	Alkyl chain vibration with TYR residue of BSA
1185	1182	Aromatic C-H in-plane deformation	1180	C-H in-plane deformation in the presence of TYR residue
1285	1280	C-C stretch of biphenyl	1283	Indicative of α helix and C-C stretching
1527	1508	C-C stretch of aromatic rings	1521	Quadrant stretching mode of the aromatic ring
1606	1605	C-C stretch of aromatic rings	1604	C-C stretch of the phenyl ring
2224	–	C ≡ N stretch	2225	C ≡ N stretch
–-	2894	$\nu_s(CH_2)$	2850;	$\nu_s(CH)$;
	-		2887	$\nu_s(CH_2)$
–	3000	Aliphatic ν(C-H)	3065	ν(C-H)

* ν-stretching; s- symmetric; as- asymmetric; β-bending; δ-deformation.

to disturbance of charge density, the linewidth broadening occurs as observed. The total integrated area is calculated where the intensities of area are calculated by averaging the areas. The intensity for all the prominent peaks observed in this spectral region sharply increases its value during the K-I phase transition of the molecules. This abrupt increase in II can be attributed to the increase in electron cloud density related to the modes.

3.3.2. Raman parameters in region of 1000–2000 cm^{-1}

In the spectral region of 1000–2000 cm^{-1}, the prominent peaks observed is assigned to the δ(C-H) of TYR residue, υ(C-C) of the biphenyl rings and vibrations related to PHE residue. In this region, we observe the Amide bands I and II consisting of υ(C = O) with the contribution of β(N-H) and υ(CN). Amide band II mainly is a combination of in-plane β (N-H) and υ(CN) with contribution from in-plane β(CO) and υ(CC) [53]. The Raman parameters can be directly related to the secondary structure of BSA, namely α-helix, β sheet and random coil in the region of 1521–1680 cm^{-1}. This bonding takes place due to the hydrogen bonding between different residues of BSA and 8CB LC.

The initial conclusion can be correlated with the analysis from docking and POM studies. The PP shows that the energy in the vibration of molecules changes with a variation of temperature. The band in this spectral region shifts its position from higher to lower frequencies during the K-I phase transition. The LW shows a sharp increase in its value as it reaches a higher temperature, as shown in Fig. 18(b)-19(b). The LW shows an increasing trend during the K-SmA phase transition. The LW shows that at 100 μM of BSA, the width is narrower in shape. The LW shows the natural lifetime limit is long. Also, the changes in the intensities of the bands show a similar pattern as in the previous spectral region, where the integrated area increases with the increase of temperature. This change in the intensities indicates the reorientation of 8CB molecules due to the conformational changes in bond formation. The band allocations for the peaks observed in this region are summarized and listed in Table 2.

3.3.3. Raman parameters in region of 2000–3300 cm^{-1}

In the spectral region of 2000–3300 cm^{-1}, the peaks at 2225 cm^{-1} are assigned to the triple bond formation of the molecules. With the increase of temperature, as seen in Fig. 13(a-b), the peak shifts its position, i.e., the peak experiences a red shift at a temperature of 22 °C. Also, the peak width is broadened from this temperature onwards, which is actually the K-SmA phase transition of the 8CB LC. Fig. 20(b) shows that the LW increases with temperature and the II area increases during the K-I phase transition. However, the other peaks observed in this region, such as 2287 cm^{-1} assigned to the $\nu_s(CH_2)$, shows a different pattern. During the SmA-I phase transition, the energy of vibration of molecules decreases with the increase of frequency (Fig. 21(a)). This change in the intensities indicates the reorientation of 8CB molecules due to the conformational changes in bond formation. The II shows that the modulation of molecular polarizability increases simultaneously with the increase in the concentration of BSA. With the increase of temperature, II increases its value during the K-I phase transition of the molecules. II also provides information

about the distribution of charges. The Raman parameters for other spectra are shown in S.I. Figs. 6-8 and their values are listed in S.I. Table 1.

The peaks observed in this region are assigned, which is summarized and listed in Table 2.

The essential characteristics observed in the interaction studies of the Raman spectra are the changes in the spectral profile and the decrease in intensities. From these changes, it can be interpreted that a disruption of the intermolecular and intramolecular occurs. These changes in the Raman spectrum on the interaction between 8CB and BSA indicate the difference in the molecular structure. The binding occurs due to the hydrogen bonding and hydrophobic interactions of the molecules. Thus, confirming the experimental findings of docking and POM with Raman spectroscopic studies. As a result, the quantity of information about the structural changes of protein and LC, the orientation of LC and the environment can be concluded from vibrational studies. This makes it a promising tool for investigating the protein-ligand interaction and detection.

4. Conclusion

Summarizing our work, we have established a fundamental detection technique for BSA by 8CB LC. The detection is developed based on the reorientation of the molecules that trigger a transition from radial to bipolar configuration easily visualized under a POM. The coating of the surface by DMOAP induced homeotropic alignment and appeared dark when observed under crossed polarizers. After the addition of BSA to the DMOAP modified 8CB surface, the transition from homeotropic to the planar alignment of the cells disrupted the LC orientation. This temperature-driven orientational transition was observed through POM and confirmed the detection of BSA by 8CB. It shows high sensitivity at a concentration of 100 μM of BSA. *In-silico* molecular docking studies determined the binding location and the efficient binding energy required to bind 8CB with the active residues of BSA. The binding location is detected at a subdomain IB with a −8.80 Kcal/mol binding energy. The experimental findings from this study depend on performing accurate docking studies with the stabilization of 8CB molecules by residues through π-alkyl, π-sigma, and alkyl interactions. Raman spectroscopic studies as a potential tool are employed to understand the structural changes and confirm the protein-ligand interactions. The binding of 8CB with BSA outcomes in the reorientation of 8CB molecules generates modifications in the intensity of Raman modes. The binding is caused by hydrogen bonding, hydrophobic and van der Waals interactions. The technique proposed here for LC-based biosensing is expected to provide insights and develop the LC molecules to achieve highly sensitive and cost-effective sensors.

CRediT authorship contribution statement

Priyanki Kalita: Data curation, Formal analysis, Investigation, Visualization, Writing – original draft. **Ranjan K. Singh:** Resources, Software. **Ayon Bhattacharjee:** Conceptualization, Data curation, Methodology, Project administration, Resources, Software, Supervision, Validation, Writing – review & editing.

Declaration of Competing Interest

The authors declare that they have no known competing financial interests or personal relationships that could have appeared to influence the work reported in this paper.

Acknowledgement

The author P. Kalita likes to thank Shashank Sekhar Shukla and Chandan Bhai Patel, Department of Physics, Banaras Hindu University, for their support in Raman spectroscopic characterization.

Appendix A. Supplementary material

Supplementary data to this article can be found online at https://doi.org/10.1016/j.saa.2022.121347.

References

[1] C. Esteves, E. Ramou, A.R.P. Porteira, A.J. Moura Barbosa, A.C.A. Roque, Seeing the unseen: the role of liquid crystals in gas-sensing technologies, Adv. Opt. Mater. 8 (11) (2020) 1902117, https://doi.org/10.1002/ADOM.201902117.
[2] G. Pirnat, M. Humar, I. Muševič, Remote and autonomous temperature measurement based on 3D liquid crystal microlasers, Opt. Express 26 (18) (2018) 22615, https://doi.org/10.1364/OE.26.022615.
[3] A.P. Dabkowska, C. Hirst, M. Valldeperas, L.A. Clifton, C. Montis, S. Nöjd, L. Gentile, M. Wang, G.K. Pálsson, S. Lages, D. Berti, J. Barauskas, T. Nylander, Temperature responsive lipid liquid crystal layers with embedded nanogels, Chem. Commu.n 53 (8) (2017) 1417–1420, https://doi.org/10.1039/C6CC09426K.
[4] Y. Liu, D. Zhao, Boundary effect on the spontaneous deformation of a liquid crystal elastomer plate with arbitrary director orientation, Phys. Rev. E 103 (2021), https://doi.org/10.1103/PhysRevE.103.012701 012701.
[5] Wani OM, Zeng H, Priimagi A. A light-driven artificial flytrap. Nat Commun 2017 81 2017;8:1–7. https://doi.org/10.1038/ncomms15546
[6] Sargazi M, Linford MR, Kaykhaii M. Liquid Crystals in Analytical Chemistry: A Review. 2018;49:243–55. https://doi.org/10.1080/10408347.2018.1512399
[7] X. Lu, X. Song, J. Du, Y. Zhang, L. Zhang, X. Xiong, Preparation of DNA-functionalized surfaces for simultaneous homeotropic orientation of liquid crystals and optical recognition of analytes: application to the determination of progesterone, Mikrochim. Acta 186 (7) (2019), https://doi.org/10.1007/S00604-019-3558-7.
[8] A.D. Price, D.K. Schwartz, DNA hybridization-induced reorientation of liquid crystal anchoring at the nematic liquid crystal/aqueous interface, J Am. Chem. Soc. 130 (26) (2008) 8188–8194, https://doi.org/10.1021/JA0774055.
[9] L.N. Tan, V.J. Orler, N.L. Abbott, Ordering transitions triggered by specific binding of vesicles to protein-decorated interfaces of thermotropic liquid crystals, Langmuir 28 (15) (2012) 6364–6376, https://doi.org/10.1021/la300108f.
[10] Y. Zhao, N. Mahaja, J. Fang, Self-assembled cylindrical lipid tubules with a birefringent core, Small 2 (3) (2006) 364–367, https://doi.org/10.1002/SMLL.200500430.
[11] D. Hartono, S.L. Lai, K.-L. Yang, L.-Y. Yung, A liquid crystal-based sensor for real-time and label-free identification of phospholipase-like toxins and their inhibitors, Biosens. Bioelectron. 24 (7) (2009) 2289–2293, https://doi.org/10.1016/j.bios.2008.11.021.
[12] P. Kalita, S.S. Shukla, R.K. Singh, A. Bhattacharjee, Potential liquid crystal-based biosensor depending on the interaction between liquid crystals and proteins, Spectrochim. Acta Part A Mol. Biomol. Spectrosc. 254 (2021) 119634, https://doi.org/10.1016/j.saa.2021.119634.
[13] T. Bera, J. Deng, J. Fang, Protein-induced configuration transitions of polyelectrolyte-modified liquid crystal droplets, J. Phys. Chem. B 118 (18) (2014) 4970–4975, https://doi.org/10.1021/jp501587h.
[14] P. Kalita, R.K. Singh, A. Bhattacharjee, Interactions investigated by the spectroscopic, microscopic and molecular docking studies for liquid crystal-based biosensor, Liq. Cryst. 49 (3) (2022) 297–311, https://doi.org/10.1080/02678292.2021.1962423.
[15] J.M. Brake, N.L. Abbott, An experimental system for imaging the reversible adsorption of amphiphiles at aqueous-liquid crystal interfaces, Langmuir 18 (16) (2002) 6101–6109, https://doi.org/10.1021/la011746t.
[16] M.I. Kinsinger, B. Sun, N.L. Abbott, D.M. Lynn, Reversible control of ordering transitions at aqueous/liquid crystal interfaces using functional amphiphilic polymers, Adv. Mater. 19 (23) (2007) 4208–4212, https://doi.org/10.1002/adma.200700718.
[17] Ul Amin N, Siddiqi HM, Lin YK, Hussain Z, Majeed N. Bovine serum albumin protein-based liquid crystal biosensors for optical detection of toxic heavy metals in water. Sensors (Switzerland) 2020;20. https://doi.org/10.3390/s20010298.
[18] Y.L. Chiang, M.J. Lee, W. Lee, Enhancing detection sensitivity in quantitative protein detection based on dye-doped liquid crystals, Dye Pigment 157 (2018) 117–122, https://doi.org/10.1016/j.dyepig.2018.04.058.
[19] G.E. Volovik, L.D. Landau, D. Lavrentovich, Topological dynamics of defects: boojums in nematic drops, JETP 58 (1983) 1159.
[20] T. Bera, J. Deng, J. Fang, Tailoring the surface of liquid crystal droplets with chitosan/surfactant complexes for the selective detection of bile acids in biological fluids, RSC Adv. 5 (86) (2015) 70094–70100, https://doi.org/10.1039/c5ra09937d.

[21] W. Khan, S.Y. Park, Configuration change of liquid crystal microdroplets coated with a novel polyacrylic acid block liquid crystalline polymer by protein adsorption, Lab Chip 12 (2012) 4553–4559, https://doi.org/10.1039/c2lc40710h.
[22] R.J. Carlton, J.T. Hunter, D.S. Miller, R. Abbasi, P.C. Mushenheim, L.N. Tan, N.L. Abbott, Chemical and biological sensing using liquid crystals, Liq. Cryst. Rev. 1 (1) (2013) 29–51, https://doi.org/10.1080/21680396.2013.769310.
[23] Niu X, Luo D, Chen R, Wang F, Sun X, Dai H. Optical biosensor based on liquid crystal droplets for detection of cholic acid 2016. https://doi.org/10.1016/j.optcom.2016.07.016
[24] J. Kim, M. Khan, S.-Y. Park, Glucose sensor using liquid-crystal droplets made by microfluidics, ACS Appl. Mater. Interfaces 5 (24) (2013) 13135–13139, https://doi.org/10.1021/am404174n.
[25] Verma I, Sidiq S, Pal SK. Protein triggered ordering transitions in poly (L-lysine)-coated liquid crystal emulsion droplets. 2019;46:1318–26. https://doi.org/10.1080/02678292.2019.1577995
[26] Manaila-Maximean D. Confined liquid crystals-polymer dispersed liquid crystal films. University Politehnica of Bucharest Scientific Bulletin-Series A-Applied Mathematics and Physics, 2021;83:271–8
[27] D.S. Kang, K.-S. Kwon, S.I. Kim, M.-S. Gong, S.S.A. Seo, T.W. Noh, S.-W. Joo, Temperature-dependent raman spectroscopic study of the nematic liquid crystal 4- n -pentyl-4′-cyanobiphenyl, Appl. Spectrosc. 59 (9) (2005) 1136–1140, https://doi.org/10.1366/0003702055012492.
[28] S. Siddhanta, C. Narayana, Surface enhanced Raman spectroscopy of proteins, Implications for Drug Designing 2 (2012) 1, https://doi.org/10.5772/46209.
[29] P. Miškovský, D. Jancura, S. Sánchez-Cortés, E. Kočišová, L. Chinsky, Antiretrovirally active drug hypericin binds the IIA subdomain of human serum albumin: resonance raman and surface-enhanced raman spectroscopy study, J. Am. Chem. Soc. 120 (1998) 6374–6379, https://doi.org/10.1021/JA974233A.
[30] D. Manaila-Maximean, G. Bossis, C. Metayer, F. Giulieri, Study of composite system: silica colloidal particles in nematic liquid crystal, Mol. Cryst. Liq. Cryst. 417 (1) (2004) 227–233, https://doi.org/10.1080/15421400490478876.
[31] M. Sadati, H. Ramezani-Dakhel, W. Bu, E. Sevgen, Z. Liang, C. Erol, M. Rahimi, N. Taheri Qazvini, B. Lin, N.L. Abbott, B. Roux, M.L. Schlossman, J.J. de Pablo, Molecular Structure of Canonical Liquid Crystal Interfaces, J. Am. Chem. Soc. 139 (10) (2017) 3841–3850, https://doi.org/10.1021/jacs.7b00167.
[32] I. Chaban, C. Klieber, R. Busselez, K.A. Nelson, T. Pezeril, Crystalline-like ordering of 8CB liquid crystals revealed by time-domain Brillouin scattering, J. Chem. Phys. 152 (1) (2020) 014202, https://doi.org/10.1063/1.5135982.
[33] M.F. Palermo, A. Pizzirusso, L. Muccioli, C. Zannoni, An atomistic description of the nematic and smectic phases of 4-n-octyl-4′ cyanobiphenyl (8CB), J. Chem. Phys. 138 (20) (2013) 204901, https://doi.org/10.1063/1.4804270.
[34] S.A. Adcock, J.A. McCammon, Molecular dynamics: survey of methods for simulating the activity of proteins, Chem. Rev. 106 (2006) 1589–1615, https://doi.org/10.1021/cr040426m.
[35] Theodore Peters J. All About Albumin. Elsevier; 1995. https://doi.org/10.1016/b978-0-12-552110-9.x5000-4.
[36] C.N. Pace, F. Vajdos, L. Fee, G. Grimsley, T. Gray, How to measure and predict the molar absorption coefficient of a protein, Protein Sci. 4 (11) (1995) 2411–2423, https://doi.org/10.1002/pro.5560041120.
[37] A.S. Roy, A.K. Dinda, N.K. Pandey, S. Dasgupta, Effects of urea, metal ions and surfactants on the binding of baicalein with bovine serum albumin, J. Pharm. Anal. 6 (4) (2016) 256–267, https://doi.org/10.1016/j.jpha.2016.04.001.
[38] Jampani V, R P. Surface coupling agent (DMOAP) for colloidal liquid crystal studies. 2000:1–17.
[39] Bujacz A. Structures of bovine, equine and leporine serum albumin. Acta Crystallogr Sect D Biol Crystallogr 2012;68:1278–89. https://doi.org/10.1107/S0907444912027047(accessed March 29, 2022).
[40] 4-Cyano-4′-octylbiphenyl | C21H25N - PubChem. https://pubchem.ncbi.nlm.nih.gov/compound/104289 (accessed March 29, 2022).
[41] Achilles Blind Docking Server. https://bio-hpc.ucam.edu/aquiles/ (accessed March 30, 2022).
[42] I. Sánchez-Linares, H. Pérez-Sánchez, J.M. Cecilia, J.M. García, High-throughput parallel blind virtual screening using BINDSURF, BMC Bioinf. 13 (S14) (2012), https://doi.org/10.1186/1471-2105-13-S14-S13.
[43] A.A.T. Naqvi, T. Mohammad, G.M. Hasan, M.I. Hassan, Advancements in docking and molecular dynamics simulations towards ligand-receptor interactions and structure-function relationships, Curr. Top Med. Chem. 18 (20) (2018) 1755–1768, https://doi.org/10.2174/1568026618666181025114157.
[44] X.-Y. Meng, H.-X. Zhang, M. Mezei, M. Cui, Molecular docking: a powerful approach for structure-based drug discovery, Curr. Comput Aided Drug Des 7 (2011) 146.
[45] J. Du, Q. Jiang, X. Lu, L. Chen, Y. Zhang, X. Xiong, Detection of sulfadimethoxine using optical images of liquid crystals, Analyst 144 (5) (2019) 1761–1767, https://doi.org/10.1039/C8AN02049C.
[46] S. Yang, C. Wu, H. Tan, Y. Wu, S. Liao, Z. Wu, G. Shen, R. Yu, Label-free liquid crystal biosensor based on specific oligonucleotide probes for heavy metal ions, Anal. Chem. 85 (1) (2013) 14–18, https://doi.org/10.1021/AC302989H.
[47] D.S. Goodsell, H. Lauble, C.D. Stout, A.J. Olson, Automated docking in crystallography: analysis of the substrates of aconitase, Proteins 17 (1) (1993) 1–10, https://doi.org/10.1002/PROT.340170104.
[48] T.N. Hart, R.J. Read, A multiple-start Monte Carlo docking method, Proteins 13 (3) (1992) 206–222, https://doi.org/10.1002/PROT.340130304.
[49] R. Wang, Y. Lu, X. Fang, S. Wang, An extensive test of 14 scoring functions using the PDBbind refined set of 800 protein−ligand complexes, J. Chem. Inf. Comput. Sci. 44 (6) (2004) 2114–2125, https://doi.org/10.1021/CI049733J.
[50] W.L. Jorgensen, D.S. Maxwell, J. Tirado-Rives, Development and testing of the OPLS all-atom force field on conformational energetics and properties of organic liquids, J. Am. Chem. Soc. 118 (45) (1996) 11225–11236, https://doi.org/10.1021/JA9621760.
[51] S. Salentin, S. Schreiber, V.J. Haupt, M.F. Adasme, M. Schroeder, PLIP: Fully automated protein-ligand interaction profiler, Nucleic Acids Res. 43 (W1) (2015) W443–W447, https://doi.org/10.1093/nar/gkv315.
[52] B. Sjöberg, S. Foley, B. Cardey, M. Enescu, An experimental and theoretical study of the amino acid side chain Raman bands in proteins, Spectrochim. Acta - Part A Mol. Biomol. Spectrosc. 128 (2014) 300–311, https://doi.org/10.1016/j.saa.2014.02.080.
[53] W.R. Premasiri, D.T. Moir, M.S. Klempner, N. Krieger, G. Jones, L.D. Ziegler, Characterization of the surface-enhanced Raman scattering (SERS) of bacteria, J. Phys. Chem. B 109 (1) (2005) 312–320, https://doi.org/10.1021/JP040442N.